J Mol Model (2012) 18:963–972
DOI 10.1007/s00894-011-1132-2

ORIGINAL PAPER

Theoretical study of crown ethers with incorporated azobenzene moiety

Yuan Miao · Xueye Wang · Dan Ouyang

Received: 17 March 2011 / Accepted: 16 May 2011 / Published online: 4 June 2011

Abstract A series of crown ethers containing the azobenzene moiety incorporated into crowns of various sizes [$Cr(O_6)$, $Cr(O_7)$ and $Cr(O_8)$] and their corresponding alkali metal cation (Li^+, Na^+, K^+, Rb^+) complexes have been studied theoretically. The density functional theory (DFT) method was employed to elucidate the stereochemical structural natures and thermodynamic properties of all of the target molecules at the B3LYP/6-31 G(d) and LANL2DZ level for the cation Rb^+. The fully optimized geometries had real frequencies, thus indicating their minimum-energy status. In addition, the bond lengths between the metal cation and oxygen atoms, atomic torsion angles and thermodynamic energies for complexes were studied. Natural bond orbital (NBO) analysis was used to explore the origin of the internal forces and the intermolecular interactions for the metal complexes. The calculated results show that the most significant interaction is that between the lone pair electrons of electron-donating oxygens in the *cis*-forms of azobenzene crown ethers (*cis*-ACEs) and the LP* (1-center valence antibond lone pair) orbitals of the alkali-metal cations (Li^+, Na^+, K^+ and Rb^+). The electronic spectra for the *cis*-ACEs [*cis*-$Cr(O_6)$, *cis*-$Cr(O_7)$ and *cis*-$Cr(O_8)$] are obtained by the time-dependent density functional theory (TDDFT) at the B3LYP/6-31 G(d) level. The spectra of the *cis*-isomers show broad $\pi \rightarrow \pi^*$ ($S_0 \rightarrow S_2$) absorption bands at 310–340 nm but weaker $n \rightarrow \pi^*$ ($S_0 \rightarrow S_1$) bands at 480–490 nm. The calculated results are in good agreement with the experimental results.

Y. Miao · X. Wang (✉) · D. Ouyang
Key Laboratory of Environmentally Friendly Chemistry and Applications of Ministry of Education, College of Chemistry, Xiangtan University,
Xiangtan, Hunan 411105, People's Republic of China
e-mail: wxueye@xtu.edu.cn

Keywords Azobenzene crown ethers (ACEs) · Photoisomerization · Preorganization · Switchable molecules · Time-dependent density functional theory (TDDFT)

Introduction

Supramolecular chemistry is a highly interdisciplinary field covering the chemical, physical, and biological features of complex chemical species that are held together and organized by means of intermolecular (noncovalent) bonding interactions. How well things fit together depends on their predisposition to do so, a matter frequently referred to as "preorganization." Reliably predicting host–guest interactions is an important goal of supramolecular chemistry [1]. A molecular system with a preorganized and effectively functionalized recognition unit for guest molecules is ideal for host–guest interactions.

Nowadays, most molecular builders are very interested in constructing switchable molecular systems that can selectively bind different metal cations. The key to designing a successful system of this type involves the use of binding interactions that have well-defined, predictable geometric consequences. These are important aspects in the development of functional molecular devices of increasing complexity [2]. Ever since the first synthesis of crown ethers was reported by Pedersen [3], these molecules have been the focus of extensive study due to their ability to complex metal cations [4]. A large number of studies have shown that the binding properties of crown ethers are sensitive to change in conformation or effective size [5].

Azobenzenes comprise an interesting class of compounds that exhibit photoresponsive properties. Their photoisomerization properties have led to them becoming

among the most common used photoresponsive molecular switches [6]. They have been incorporated into a number of supramolecular frameworks to produce ionophores for transports and photoswitchable receptors [7]. Azobenzene has the ability to undergo isomerization between the straight *trans*-isomer and the bent *cis*-isomer with light irradiation (*trans* ↔ *cis*) and thermal induction (*cis* → *trans*) (see Fig. 1), respectively. Because of their facile interconversion at appropriate wavelengths, azobenzenes have the potential to be used in optical switching and image storage devices [8–11] as well as molecular scissors [12] and as targets for coherent control in molecular electronics [13].

The basic requirement of a successful molecular switch is the presence of two distinct forms of the molecule that can be interconverted reversibly by means of an external stimulus, such as light, heat, pressure, magnetic or electric fields, a pH change or a chemical reaction [14]. Irradiating or heating azobenzene-containing materials induces reversible isomerization between the two isomers, making azobenzenes switchable molecules. The isomerization of azobenzenes is accompanied by significant changes in the absorption spectra and structures of the molecules. These changes can alter properties of their surrounding environment by switching them "on" or "off."

The azobenzene moiety incorporated into the crowns (see Fig. 2) is used to change the size of the crowns and hence to modify the complexing properties of the molecules [15, 16]. The combination of a crown ether with an azobenzene moiety enables us to control ionic conductivity by light irradiation or thermal induction.

The azobenzene-type crown ethers (hereafter referred to as "ACEs") $Cr(O_7)$ and $Cr(O_8)$, in which the 4 and 4′ positions of azobenzene are linked by a polyoxyethylene chain, were synthesized and studied by Seiji Shinkai and co-workers [17]. $Cr(O_7)$ and $Cr(O_8)$ have azobenzene as an antenna and the crown ether as a functional group, and change their chemical and physical functions in response to photoirradiation or changes in temperature. Similarly, azobenzene derivatives have been utilized as light-driven or temperature-driven triggers to control the functions of metal ligands.

Computational methods are a promising way to calculate the structures and properties of complexes, such as their binding energies and absorbance spectra. In the work presented here, a family of ACEs [$Cr(O_6)$, $Cr(O_7)$ and $Cr(O_8)$] with rings of different sizes containing the azobenzene moiety incorporated into the crown were studied theoretically.

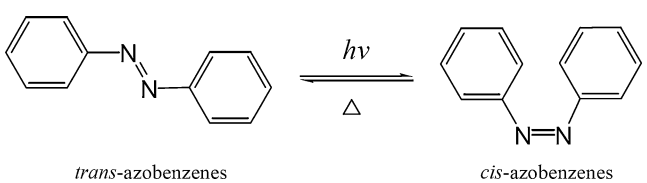

Fig. 1 Schematic diagram of the *trans* ↔ *cis* isomerization of azobenzenes

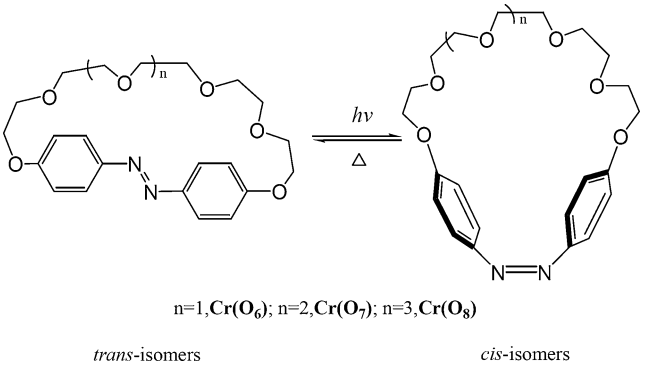

Fig. 2 Schematic diagram of the *trans* ↔ *cis* isomerization of crown ethers with an incorporated azobenzene moiety

Theory and methods of calculation

In the framework of the density functional theory (DFT) approach, the B3LYP hybrid functional [18, 19] is one of the most preferred methods, as it has proven its ability to reproduce various molecular properties, including structural parameters and vibrational spectra. The combined use of the B3LYP functional and the standard split valence basis set 6-31 G(d) has been previously shown to provide an excellent compromise between the accuracy of the results and computational efficiency for large and medium-sized molecules [20–26]. Ground-state electronic structure calculations of all complexes were performed using density functional theory (DFT) methods as implemented using the Gaussian 03 software package [27]. The functional that was used throughout this study is B3LYP, consisting of a hybrid exchange functional, as defined by Becke's three-parameter equation, and the Lee–Yang–Par correlation functional [18, 19]. The ground-state geometries were obtained in the gas phase by full geometry optimization, and the optimum structures, located as stationary points on the potential energy surfaces, were verified by the absence of imaginary frequencies. The standard 6–31 G(d) and LANL2DZ basis sets were found to be suitable for most ligands.

Time-dependent density functional theory (TDDFT) can model highly complex molecules like azobenzenes accurately, efficiently, and cost-effectively. In this study, TDDFT was used to model the absorption spectra of several azobenzene derivatives. The results show a reasonably good association between the theoretical and experimental values for the absorbance spectra of the azobenzenes. A natural bond orbital (NBO) population analysis was performed with the NBO 3.1 program as implemented in Gaussian [28–31]. NBO analysis represents a unique and powerful approach to evaluating the

origins of intermolecular interactions from a computational standpoint.

The binding energies, binding enthalpies, and Gibbs free energies in the gas phase for the complexes were calculated for the reaction

$$cis-\mathrm{ACEs}_{\mathrm{free}}+\mathrm{M}^{+}_{\mathrm{free}}\rightarrow(cis-\mathrm{ACEs}/\mathrm{M}^{+})_{\mathrm{complex}}. \quad (1)$$

For this system, the binding energy ΔE can be expressed as follows:

$$\Delta E=E(cis-\mathrm{ACEs}/\mathrm{M}^{+})_{\mathrm{complex}}-[E(cis-\mathrm{ACEs}_{\mathrm{free}})+E(\mathrm{M}^{+}_{\mathrm{free}})]. \quad (2)$$

Results and discussion

Optimized ground-state geometry

The structures of molecules play an especially important role in determining their chemical properties. The optimized stability structures for both the *trans* and *cis* forms of ACEs [$Cr(O_6)$, $Cr(O_7)$ and $Cr(O_8)$] were obtained at the B3LYP/6-31 G(d) level in the gas phase at 298 K, while unsubstituted *trans*- and *cis*-azobenzene were studied as reference compounds at the same level. The results of the analysis of all of the target molecules described above are depicted in Table 1, and their ground-state structures are presented in Fig. 3.

The *trans* isomer of azobenzene is about 15.1 kcal mol^{-1} or 0.65 eV lower in energy than that of the *cis* isomer. This is only slightly higher than the experimental value of 0.6 eV [32]. The DFT results are very similar to some of the previous theoretical predictions [33–39]. The calculated results indicate that the phenyl rings of *trans*-azobenzene are 50.2° out of plane compared to those of the *cis* isomer, and the distance between the 4 and 4′ positions decreases from 9.079 Å to 6.562 Å for *trans*- and *cis*-azobenzene, respectively.

The energies of the *cis* ACEs are 16.3 kcal mol^{-1} (*cis*-Cr(O_6)), 20.1 kcal mol^{-1} (*cis*-Cr(O_7)), and 15.7 (*cis*-Cr(O_8)) kcal mol^{-1} higher than those of their corresponding *trans* isomers, respectively. The optimized structures of the *trans* isomers of Cr(O_6), Cr(O_7), and Cr(O_8) are shown in Fig. 3, and the calculated parameters for them are listed in Table 1. The polyoxyethylene $(-CH_2-O-CH_2-)_n$ (n=1, 2, 3) chains between the two aromatic rings are almost linearly extended. The distances between the 4 and 4′ positions of azobenzene of the three *trans* isomers are 8.945, 9.072 and 9.034 Å, respectively, which are all smaller than those of the unsubstituted *trans*-azobenzene (9.079 Å). The angle ∠NNCC for *trans*-Cr(O_6), *trans*-Cr(O_7), and *trans*-Cr(O_8) are 3.2°, 1.4°, and 8.4°, respectively. These results indicate that the phenyl rings of the *trans*-azobenzene unit in the ACEs are out of plane compared to those of the unsubstituted azobenzene, and there must be some steric restriction in play during the *trans* ↔ *cis* isomerization. The methylene chain of *trans*-Cr(O_8) undergoes a small amount of folding, and *trans*-Cr(O_6) shows the most restricted structure (see from Fig. 3). The *trans* isomers of the ACEs show poor preorganization because of the long loops in their structures; the isomers lack any affinity for metal cations according to the rules of supermolecule preorganization [40]. With respect to the *cis* ACEs, there is a crown loop in each of the target molecules. The preorganization of the *cis* forms of ACEs is enhanced, allowing them to coordinate with metal cations; they thus present an "on" state, while the *trans* forms of the ACEs are in an "off" state in terms of coordinating with metal cations. *Cis* forms of these crown ethers show affinity for metal cations. The sizes of the loops in the *cis*-type ACEs follows the order: *cis*-Cr(O_6)<*cis*-Cr(O_7)<*cis*-Cr(O_8). The arrangement of atoms in

Table 1 Comparison of the calculated parameters of the *trans* and *cis* isomers of ligands optimized at the B3LYP/6-31 G(d) level

Ligand	Angle (°)		Distances (Å)				Energy[a] (kcal/mol)
	∠CNNC	∠NNCC	∠NNC	d_{NN}	d_{CN}	d_{C-C}	
Trans-azobenzene	180.0	0	114.8	1.261	1.419	9.079	0
Cis-azobenzene	9.8	50.2	124.1	1.250	1.436	6.562	15.1
Trans-Cr(O_6)	171.0	3.2	114.8	1.265	1.410	8.945	0
Cis-Cr(O_6)	11.1	49.6	123.6	1.253	1.434	6.507	16.3
Trans-Cr(O_7)	176.8	1.4	115.3	1.265	1.410	9.072	0
Cis-Cr(O_7)	9.0	57.2	122.4	1.254	1.434	6.233	20.1
Trans-Cr(O_8)	178.0	8.4	113.5	1.264	1.408	9.034	0
Cis-Cr(O_8)	8.3	48.6	123.5	1.255	1.434	6.284	15.7

d_{C-C}: the distances (Å) between the 4 and 4′ positions of azobenzene and azobenzene crown ethers (ACEs)

[a] Energies are relative to the corresponding *trans* isomer of the ligand

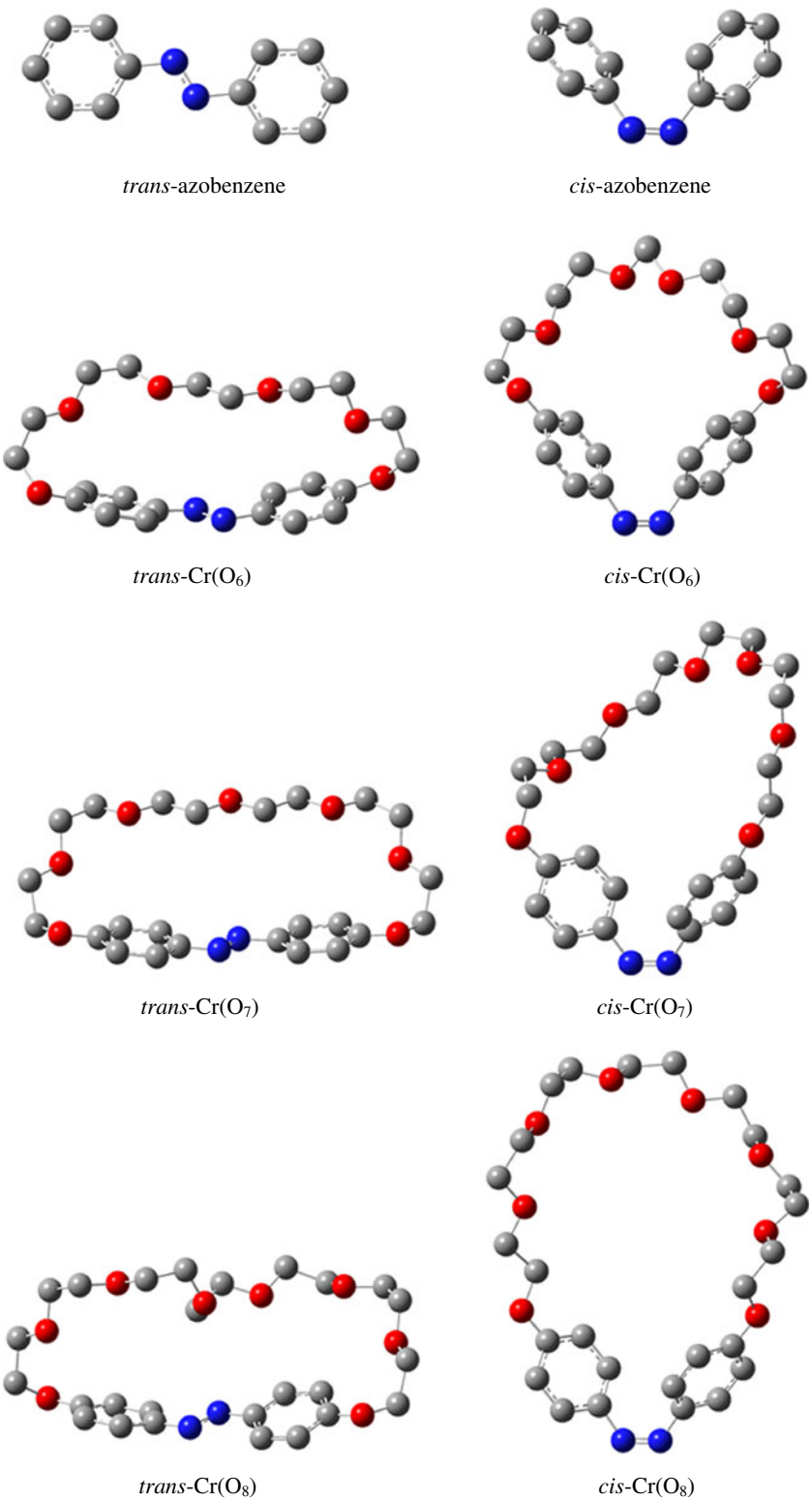

Fig. 3 The optimized structures of the *trans* and *cis* isomers of azobenzene and azobenzene crown ethers (ACEs) at the B3LYP/6-31 G(d) level

the *cis* isomers is more relaxed than that in the *trans* isomers. In addition, the flexibility of the crown-like loop increases as the number of $–CH_2–O–CH_2–$ units between the 4 and 4′ positions of azobenzene increases. These results show that in ACEs with a polyoxyethylene chain, the crown-like loop appears in *cis* ACEs and disappears in *trans* ACEs, causing an "all-or-nothing" change in the ion-binding ability. The molecules of ACEs in their *cis* and *trans* isomer forms act as "switched-on" and "switched-off" crown ethers, respectively.

Optimized geometries of the complexes

The optimized structures of the *cis* ACE/M^+ complexes [*cis*-Cr(O_6), *cis*-Cr(O_7) and *cis*-Cr(O_8)]/Li^+, Na^+, K^+ and Rb^+] are given in Fig. 4, whereas the most important parameters for these complexes, which were optimized by performing DFT at the B3LYP/6-31 G(d) and LANL2DZ level, are given in Table 2.

Upon inspecting Figs. 3 and 4 and Tables 1 and 2, it is clear that the distances between the 4 and 4′ positions of the

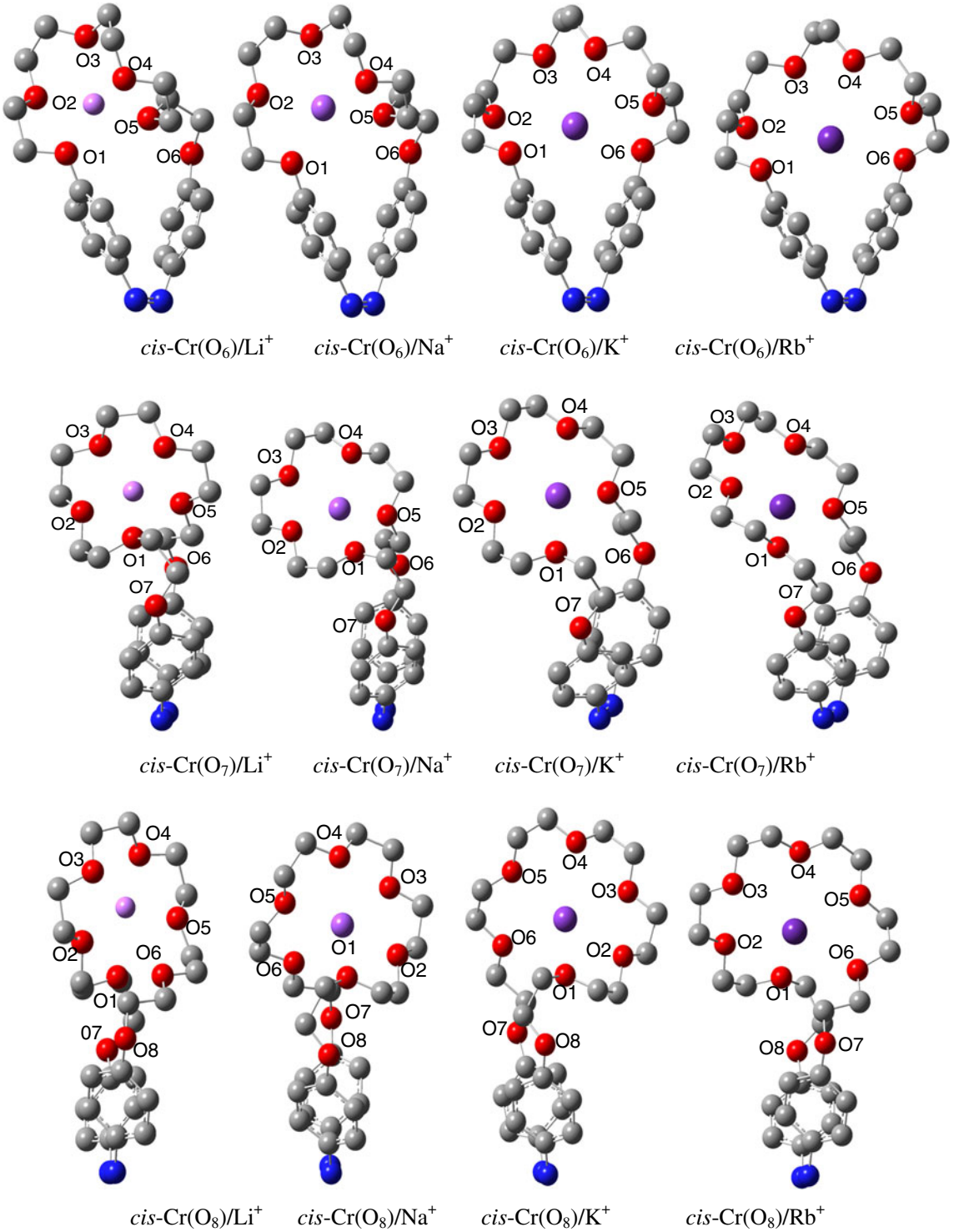

Fig. 4 The optimized structures of the *cis* isomers of azobenzene crown ethers (*cis* ACEs) complexed with Li^+, Na^+, K^+ and Rb^+ metal cations, obtained at the B3LYP/6-31 G(d) and LANL2DZ level of theory

Table 2 Selected parameters for the ACE/M^+ (Li^+, Na^+, K^+ and Rb^+) complexes optimized at the B3LYP/6-31 G(d) and LANL2DZ level (distances in Å, dihedral angles in degrees °)

Parameter	*cis*-Cr(O_6)				*cis*-Cr(O_7)					*cis*-Cr(O_8)		
	Li^+	Na^+	K^+	Rb^+	Li^+	Na^+	K^+	Rb^+	Li^+	Na^+	K^+	Rb^+
r_1	2.155	2.405	3.370	3.709	2.105	2.413	2.796	3.137	3.290	2.675	2.934	3.065
r_2	2.096	2.431	2.909	3.125	2.044	2.424	2.777	2.983	2.009	2.380	2.752	2.969
r_3	2.343	2.486	2.864	3.027	2.193	2.470	2.776	3.015	2.055	2.511	2.843	3.012
r_4	2.078	2.387	2.864	3.027	1.989	2.372	2.753	3.020	2.066	2.518	2.841	3.006
r_5	2.094	2.457	2.907	3.125	2.226	2.439	2.813	3.097	2.016	2.363	2.781	2.983
r_6	4.965	5.115	3.357	3.709	_	_	_	_	3.192	2.585	2.935	3.131
d_{C-C}	5.027	5.307	5.365	5.814	5.663	5.530	5.870	5.915	6.391	5.606	5.391	5.689
∠CNNC	7.0	7.7	7.5	8.6	8.3	7.3	8.4	8.5	8.5	8.1	6.7	8.4
∠NNCC	64.3	62.9	65.6	64.5	59.5	57.7	54.8	52.7	55.1	61.0	57.7	58.4

r: bond lengths (Å) between O atoms and alkali-metal cations

d_{C-C}: distances (Å) between the 4 and 4′ positions of azobenzene

azobenzene crown ether loops all change greatly when the free ligand *cis* ACE [*cis*-Cr(O_6), *cis*-Cr(O_7) and *cis*-Cr(O_8)] coordinates with the alkali cations (Li^+, Na^+, K^+ and Rb^+). It can be assumed that the decreased distances d_{C-C} are due to the inductive effect arising from the O…M^+ interactions. The smaller the number of methylene groups between the 4 and 4′ positions of azobenzene, the stronger the restrictions on the crown-like ring. In addition, not all of the oxygen atoms can contribute to the formation of a crown-like ring in the *cis* isomers. The oxygen atoms in the crown loops do not all interact with M^+(Li^+, Na^+, K^+ and Rb^+) because they are too far away.

When the crown ether loop of *cis*-Cr(O_6) coordinates with an alkali-metal cation, the structural features of the dihedral angle ∠CNNC of the complex change significantly and show different properties to those of the metal-free *cis*-Cr(O_6) (11.1°). Upon inspecting Fig. 4 and Table 2, it is clear that in the complexes *cis*-Cr(O_6)/Li^+ and *cis*-Cr(O_6)/Na^+, the interatomic distances between Li^+ and (O_1–O_6) are 2.155, 2.096, 2.343, 2.078, 2.094, and 4.965 Å; those between Na^+ and (O_1–O_6) are 2.405, 2.431, 2.486, 2.387, 2.457, and 5.115 Å, respectively. It is clear that r_6 is 4.965 Å for *cis*-Cr(O_6)/Li^+ and 5.115 Å for *cis*-Cr(O_6)/Na^+. The bond length r_6 is much larger than the others in each of the complexes. The oxygen O_6 in the crown loop of *cis*-Cr(O_6) shows only weak interactions with Li^+ and Na^+ because it is too far away from them. The optimized structure of *cis*-Cr(O_6) with and without the cations K^+ and Rb^+ presents only small changes. This result can be attributed to the small size of the crown-like cavity but the big cation diameters of K^+ and Rb^+.

Turning our attention to the structures of the complexes *cis*-Cr(O_7)/M^+ (Li^+, Na^+, K^+ and Rb^+), a polyoxyethylene loop is formed that is analogous to 15-crown-5 [40–42]. Not all of the donor oxygen atoms in *cis*-Cr(O_7) interact with metal cations. In the complexes, the average coordination bond lengths of the metal cations are 2.111, 2.424, 2.783, and 3.050 Å, respectively. The bond lengths for *cis*-CrO_7/Li^+ and Na^+ are smaller than those for *cis*-Cr(O_7)/K^+ and Rb^+; in other words, there are stronger metal–oxygen interactions between the ligand *cis*-Cr(O_7) and Li^+ and Na^+ than K^+ and Rb^+. Li^+ gives a shorter bond length with the donor O than Na^+ does in these complexes. However, the structures of *cis*-Cr(O_7)/M^+ (Li^+ and Na^+) from Fig. 4 indicate that Na^+ improves the planarity of the oxygens compared to Li^+. Therefore, Na^+ fits with the crown-like ring better than Li^+. *Cis*-Cr(O_7) cannot bind well with the large alkali metal cation Rb^+, as can be seen from the structures in Fig. 4.

Based on the optimized structures of the complexes formed by the alkali cations Li^+, Na^+, K^+ and Rb^+ and the ligand *cis*-Cr(O_8), a 18-crown-6 crown-like ring is produced when *cis*-Cr(O_8) coordinates with metal cations. There are six donor oxygens that are mainly involved in the O…M^+ interactions. *Cis*-Cr(O_8) can bind with both small and large alkali-metal cations, as can be seen from the structures shown in Fig. 4. Li^+ is too small to coordinate with all six oxygen atoms in the crown-like ring of *cis*-Cr(O_8). The coordination bond lengths shown in Table 2 for the complex *cis*-Cr(O_8)/Li^+ are 3.290, 2.009, 2.055, 2.066, 2.016 and 3.192 Å, respectively. It is clear that r_1 and r_6 are all much larger than the other bond lengths. The optimized structure shown in Fig. 4 indicates that Li^+ is drawn to one side of the crown-like ring. The bond lengths indicate that the best match for the crown-like loop in the ligand *cis*-Cr(O_8) is Na^+ according to the lock-and-key complementarity rule [43]. However, crown-6 ethers are known to prefer K^+ according to experimental results [44–47]. The most

plausible reason for this difference between experiment and theory is that the calculations do not include the effect of the solvent, and Na^+ is even more strongly solvated than K^+ [48]; the calculations were performed for isolated molecules in the gas phase, but the experiments were done in aqueous solution.

Natural bond orbital analysis

For each donor NBO (i) and acceptor NBO (j), the stabilization energy (E_2) associated with $i \rightarrow j$ delocalization is explicitly estimated using the following equation [49–52]:

$$E_2 = \Delta E_{ij} = q_i \frac{F^2(i,j)}{\varepsilon_j - \varepsilon_i}, \quad (3)$$

where q_i is the ith donor orbital occupancy, ε_i and ε_j, are the diagonal elements (orbital energies), and $F(i, j)$ are the off-diagonal elements, respectively, associated with the NBO Fock matrix.

The results of second-order perturbation theory analysis of the Fock matrix for *cis*-ACE/M^+ [*cis*-Cr(O_6), *cis*-Cr(O_7) and *cis*-Cr(O_8)/Li^+, Na^+, K^+ and Rb^+], obtained by NBO analysis, are summarized in Table 3. The interaction energies E_2 of the host–guest molecules *cis*-ACE/M^+ are mainly dependent on the lone-pair electrons of O atoms of the crown ether and the LP* orbitals of the alkali-metal cation (Li^+, Na^+, K^+ and Rb^+); the N atoms in the azobenzene part do not appear to be as important.

For the complexes *cis*-Cr(O_6)/M^+, the strong donor–acceptor interactions for *cis*-Cr(O_6)/Li^+ between the lone-pair electrons of the electron-donating oxygens O_1, O_2, O_3, O_4, and O_5 and the LP* orbital of Li^+ have stabilization energies of 3.05, 4.76, 4.47, 3.81, and 4.41 kcal mol^{-1}, respectively, which are much bigger than the corresponding energies E_2 for the complex *cis*-Cr(O_6)/Na^+ (1.28, 3.72, 3.14, 2.92, and 3.32 kcal mol^{-1}). Obviously, one of the electron-donating oxygens, O_6, in the ligand *cis*-Cr(O_6) is not considered to interact with Li^+ and Na^+, and the E_2 data show a poor distribution. However, the interaction stabili-

Table 3 Results of second-order perturbation theory analysis of the Fock matrix for *cis*-ACE/M^+ [*cis*-Cr(O_6), *cis*-Cr(O_7) and *cis*-Cr(O_8)/Li^+, Na^+, K^+ and Rb^+] within the NBO basis

cis-Cr(O_6)		*cis*-Cr(O_7)		*cis*-Cr(O_8)	
Donor NBO(i) →Acceptor NBO (j)	E_2 (kcal/mol)	Donor NBO(i) →Acceptor NBO (j)	E_2 (kcal/mol)	Donor NBO(i) →Acceptor NBO (j)	E_2 (kcal/mol)
LP O_1→LP* Li	3.05	LP O_1→LP* Li	4.91	LP O_1→LP* Li	3.10
LP O_2→LP* Li	4.47	LP O_2→LP* Li	4.52	LP O_2→LP* Li	3.54
LP O_3→LP* Li	4.41	LP O_3→LP* Li	4.48	LP O_3→LP* Li	3.29
LP O_4→LP* Li	3.81	LP O_4→LP* Li	4.01	LP O_4→LP* Li	3.30
LP O_5→LP* Li	4.76	LP O_5→LP* Li	5.01	LP O_5→LP* Li	3.51
				LP O_6→LP* Li	2.33
LP O_1→LP* Na	1.28	LP O_1→LP* Na	3.32	LP O_1→LP* Na	4.43
LP O_2→LP* Na	3.14	LP O_2→LP* Na	2.77	LP O_2→LP* Na	2.83
LP O_3→LP* Na	3.32	LP O_3→LP* Na	2.81	LP O_3→LP* Na	3.53
LP O_4→LP* Na	2.92	LP O_4→LP* Na	2.65	LP O_4→LP* Na	3.62
LP O_5→LP* Na	3.72	LP O_5→LP* Na	3.35	LP O_5→LP* Na	2.82
				LP O_6→LP* Na	4.18
LP O_1→LP* K	1.12	LP O_1→LP* K	2.45	LP O_1→LP* K	2.95
LP O_2→LP*K	2.36	LP O_2→LP*K	2.16	LP O_2→LP*K	2.38
LP O_3→LP* K	2.99	LP O_3→LP* K	2.01	LP O_3→LP* K	2.69
LP O_4→LP* K	2.99	LP O_4→LP* K	1.88	LP O_4→LP* K	2.72
LP O_5→LP* K	2.36	LP O_5→LP* K	2.55	LP O_5→LP* K	2.51
LP O_6→LP* K	1.11			LP O_6→LP* K	2.99
LP O_1→LP* Rb	0.57	LP O_1→LP* Rb	1.15	LP O_1→LP* Rb	1.62
LP O_2→LP* Rb	1.21	LP O_2→LP* Rb	1.03	LP O_2→LP* Rb	1.32
LP O_3→LP* Rb	1.64	LP O_3→LP* Rb	1.04	LP O_3→LP* Rb	1.51
LP O_4→LP* Rb	1.64	LP O_4→LP* Rb	1.02	LP O_4→LP* Rb	1.54
LP O_5→LP* Rb	1.21	LP O_5→LP* Rb	1.05	LP O_5→LP* Rb	1.34
LP O_6→LP* Rb	0.57			LP O_6→LP* Rb	1.76

zation energy E_2 between an electron-donating oxygen and K^+ or Rb^+ is weaker than that for *cis*-$Cr(O_6)/M^+$ (Li^+ and Na^+). Also, six electron-donating oxygens in *cis*-$Cr(O_6)$ all interact with the cations K^+ and Rb^+. This result can be attributed to the small size of the crown-like cavity and the big cation diameters of K^+ and Rb^+.

In *cis*-$Cr(O_7)/M^+$ (Li^+, Na^+, K^+ and Rb^+) complexes, the stronger donor–acceptor interactions mainly derive from the lone-pair electrons of the five electron-donating oxygens (O_1, O_2, O_3, O_4, O_5) and the LP* orbital of the alkali-metal cation M^+(Li^+, Na^+, K^+ or Rb^+), and the interaction phenomenon is analogous to 15-crown-5/M^+. The stabilization energies E_2 for the complexes *cis*-$Cr(O_7)/Li^+$ and Na^+ are larger than those of the complexes *cis*-$Cr(O_7)/K^+$ and Rb^+. For the complex *cis*-$Cr(O_7)/Li^+$, the data distribution for the stabilization energy E_2 of *cis*-$Cr(O_7)/Na^+$ is better than that of *cis*-$Cr(O_7)/Li^+$.

In the *cis*-$Cr(O_8)/M^+$ complexes, the strongest donor–acceptor interactions mainly come from the lone-pair electrons of the six electron-donating oxygens (O_1, O_2, O_3, O_4, O_5, O_6) and the LP* orbital of the alkali-metal cation M^+(Li^+, Na^+, K^+ or Rb^+), and the interaction phenomenon is analogous to 18-crown-6/M^+. The stabilization energy E_2 for O_6…Li^+ in the *cis*-$Cr(O_8)/Li^+$ complex is 2.33 kcal mol^{-1}, which is much smaller than those of the other five oxygens (O_1: 3.10, O_2: 3.54, O_3: 3.29, O_4: 3.30, O_5: 3.51 kcal mol^{-1}). The data distributions of the stabilization energies E_2 for the complexes *cis*-$Cr(O_8)/K^+$ and *cis*-$Cr(O_8)/Rb^+$ are better than those of the complexes *cis*-$Cr(O_8)/Li^+$ and *cis*-$Cr(O_8)/Na^+$. In the complex *cis*-$Cr(O_8)/K^+$, the strong donor–acceptor interactions between the lone-pair electrons of the electron-donating oxygens O_1–O_6 and the LP* orbital of Li^+ have stabilization energies of 2.95, 2.38, 2.69, 2.72, 2.51 and 2.99 kcal mol^{-1}, respectively, which are much bigger than the corresponding stabilization energies E_2 of the complex *cis*-$Cr(O_8)/Rb^+$ (1.62, 1.32, 1.51, 1.54, 1.34 and 1.76 kcal mol^{-1}).

Binding energies and stabilities

The calculated binding energies (ΔE^b), enthalpies (ΔH^b) and Gibbs free energies (ΔG^b) (298 K) of the ACE/M^+ complexes [*cis*-$Cr(O_6)$, *cis*-$Cr(O_7)$, and *cis*-$Cr(O_8)/Li^+$, Na^+, K^+ and Rb^+], based on reaction (1) at the B3LYP/6-31 G(d) and LANL2DZ level in the gas phase are listed in Table 4. When performing such a study, it is important to consider the large basis set superposition error (BSSE), which in most cases leads to overestimated interaction energies [53, 54]. One of the most commonly used methods of correcting for the BSSE is the counterpoise (CP) method [55]. Thus, the binding energies were corrected for the undesirable effects of the BSSE using the CP method at the B3LYP/6-31 G (d) level with relaxed fragment geometries.

Table 4 shows that the gas-phase binding energies (ΔE^b), binding enthalpies (ΔH^b) and Gibbs free energies (ΔG^b) at 298 K decrease for the three different free ligands *cis*-$Cr(O_6)$, *cis*-$Cr(O_7)$ and *cis*-$Cr(O_8)$ as the size of the alkali cation increases, in other words: $\Delta E_{ACEs/Li^+} > \Delta E_{ACEs/Na^+} > \Delta E_{ACEs/K^+} > \Delta E_{ACEs/Rb^+}$.

For *cis*-$Cr(O_6)/M^+$ (Li^+, Na^+, K^+ and Rb^+), the crown-like cavity ring of *cis*-$Cr(O_6)$ must undergo considerable folding/twisting to bring the binding sites in close proximity to the small cations Li^+ and Na^+. These distortions enhance the host–guest intramolecular interactions. Although the backbone of the complex suffers much distortion and displays poor structural symmetry, the calculations are performed for isolated molecules in the gas phase (i.e., they do not include the intramolecular interactions of the studied complexes); therefore, the thermal energies of *cis*-$Cr(O_6)/Li^+$ and *cis*-$Cr(O_6)/Na^+$ are larger than those of *cis*-$Cr(O_6)/K^+$ and *cis*-$Cr(O_6)/Rb^+$. However, because the

Table 4 Calculated binding energies ΔE^b (kcal mol^{-1}), binding enthalpies ΔH^b (kcal mol^{-1}), and Gibbs free energies ΔG^b (kcal mol^{-1}) in the gas phase for the complexes at 298 K

Ligands	Metal cations	ΔE^b	E_{BSSE}	$\Delta E^b{}_{BSSE}$	ΔH^b	ΔG^b
Cis-$Cr(O_6)$	Li^+	−92.9	28.9	−64.0	−93.5	−77.8
	Na^+	−72.2	22.0	−50.2	−72.8	−60.9
	K^+	−51.5	17.6	−33.9	−52.1	−41.4
	Rb^+	−23.2	13.8	−9.4	−33.9	−13.2
Cis-$Cr(O_7)$	Li^+	−105.4	18.2	−87.2	−106.0	−94.8
	Na^+	−83.5	18.2	−65.3	−84.1	−73.4
	K^+	−60.9	6.9	−54.0	−61.5	−51.5
	Rb^+	−30.7	8.2	−22.5	−31.4	−21.3
Cis-$Cr(O_8)$	Li^+	−109.8	15.1	−94.7	−110.4	−97.9
	Na^+	−90.4	14.4	−66.0	−91.0	−79.1
	K^+	−67.1	8.2	−58.9	−67.8	−58.45
	Rb^+	−33.3	6.9	−26.4	−33.9	−23.2

metal cations K^+ and Rb^+ are large but the crown-like cavity is small, the thermal energies of *cis*-Cr(O_6)/K^+ and *cis*-Cr(O_6)/Rb^+ are also small. For *cis*-Cr(O_7)/M^+ and *cis*-Cr(O_8)/M^+ (Li^+, Na^+, K^+ and Rb^+), the complexes suffer much distortion, display poor structural symmetry and so exhibit the biggest thermal energies for the cation Li^+. Thus, the relationship between the cavity size of the crown ether and the cation diameter plays an important role in determining the thermal energies of complexes during coordination.

For *cis*-Cr(O_6)/M^+, *cis*-Cr(O_7)/M^+ and *cis*-Cr(O_8)/M^+ (Li^+, Na^+, K^+ and Rb^+), the different alkali cations show different trends. If we consider Na^+, the thermal energy shows the relation *cis*-Cr(O_6)/Na^+ < *cis*-Cr(O_6)/Na^+ < *cis*-Cr(O_6)/Na^+, while the binding energies of the *cis* ACEs with Na^+ [*cis*-Cr(O_6) < *cis*-Cr(O_7) < *cis*-Cr(O_8)] indicate that the affinities of the *cis* ACEs for Na^+ increase as the number of $-CH_2-O-CH_2-$ units increases, enlarging the crown-like loop. As the loop enlarges, the rigidity of the crown ether is reduced, so it becomes easier for the ACE to bind with metal cations.

Absorption spectra

The absorption spectra of the *cis* isomers of azobenzene and ACEs [*cis*-Cr(O_6), *cis*-Cr(O_7) and *cis*-Cr(O_8)] were investigated by time-dependent density functional theory (TDDFT) with the 6-31 G(d) basis set. The calculated excitation energies (E_g), wavelengths of peak absorption (λ_{abs}) and the oscillator strengths (f) of all compounds in their optimized ground-state geometries are summarized in Table 5.

The absorption spectrum of *cis*-azobenzene shows two distinct bands: a strong $\pi\rightarrow\pi^*$,($S_0\rightarrow S_2$) absorption band peaking at about 270 nm and a much weaker $n\rightarrow\pi^*$($S_0\rightarrow S_1$) band with a peak at around 470 nm. The results are in a good agreement with some of the previous studies [56, 57].

Obviously, the values of the parameters of the *cis* isomers of the ACEs are all different from those of *cis*-azobenzene. The spectra of the *cis* ACEs [*cis*-Cr(O_6), *cis*-Cr(O_7) and *cis*-Cr(O_8)] contain broad $\pi\rightarrow\pi^*$ ($S_0\rightarrow S_2$) absorption bands with a characteristic peak at 310–340 nm in the near-UV region, and their oscillator strengths are much more intense. Weaker bands in the visible region (peak wavelengths: 480–490 nm) and lower oscillator strengths due to the $n\rightarrow\pi^*$ ($S_0\rightarrow S_1$) transitions are also observed. The spectra of the *cis* ACEs present significant redshifts in comparison to the spectrum of unsubstituted *cis*-azobenzene. This result indicates that the size of the crown has a distinct influence on the absorption spectra of the *cis* ACEs.

In ref. [15], the experimental results indicated that both Cr(O_7) and Cr(O_8) give high yields of the *cis* isomer at about 360 nm, which is a little different from the peak wavelengths obtained in our calculations. This difference between the theoretical calculations and the experimental results arises because the calculations performed in this paper relate to the gas phase at 303 K, while the experiments were performed in liquids at 298 K. However, this theoretical study is still useful for predicting reactions and gauging trends.

Conclusions and perspectives

The ground-state electronic structures of azobenzene crown ethers [ACEs: Cr(O_6), Cr(O_7) and Cr(O_8)] and complexes of their *cis* isomers with the alkali-metal cations Li^+, Na^+, K^+ and Rb^+ were obtained by DFT methods at the B3LYP/6-31 G(d) level and LANL2DZ. The significant structural differences between the optimized *trans* and *cis* isomers of the ACEs indicate that the preorganization of the *trans* ACEs is poor and in an "off" state, while it is enhanced for the *cis* isomers and in an "on" state in relation to coordinating with alkali metal cations. These "molecular machines" can therefore be used as "on/off" switches as they can switch between different molecular structures and parameters. The *cis* isomers showed spherical recognition patterns in the binding of alkali-metal cations. In NBO

Table 5 Electronic transition data obtained by TDDFT for a family of azobenzene-type crown ethers [*cis*-Cr(O_6), *cis*-Cr(O_7) and *cis*-Cr(O_8)]

Ligands	Electronic transitions	TD-B3LYP/6-31 G(d) // LANL2DZ		
		E_g (eV)	Wavelength (nm)	f
Cis-azobenzene	$S_0\rightarrow S_1$	2.60	465.30	0.0105
	$S_0\rightarrow S_2$	4.65	266.79	0.5858
Cis-Cr(O_6)	$S_0\rightarrow S_1$	2.49	497.71	0.0708
	$S_0\rightarrow S_2$	3.74	331.24	0.1951
Cis-Cr(O_7)	$S_0\rightarrow S_1$	2.57	482.33	0.0542
	$S_0\rightarrow S_2$	3.97	312.69	0.1289
Cis-Cr(O_8)	$S_0\rightarrow S_1$	2.53	490.81	0.0582
	$S_0\rightarrow S_2$	3.78	328.25	0.1370

analysis, the main intermolecular charge-transfer interactions were between the LP* orbitals of the metal cations and the lone-pair electrons of the electron-donating O atoms of the *cis* ACEs, but not all of the donor oxygen atoms in the *cis* ACEs interact with metal cations. The interaction pattern of *cis*-CrO_7 with metal cations (M^+) is analogous to 15-crown-5/M^+, while that for *cis*-$Cr(O_8)/M^+$ is analogous to 18-crown-6/M^+. A time-dependent density functional theory (TDDFT) study of the *cis* ACEs afforded their absorption spectral parameters. The results of the TDDFT study indicate that the *cis* isomers have broad $\pi \rightarrow \pi^*$ ($S_0 \rightarrow S_2$) absorption bands but weaker $n \rightarrow \pi^*$ ($S_0 \rightarrow S_1$) bands, and good agreement between the theoretical and experimental values was seen.

Acknowledgments The author wish to acknowledge the financial support from the Scientific Research Fund of Hunan Provincial Education Department (no. 09A091).

References

1. Kyba EP, Helgeson RC, Madan K, Gokel GW, Tarnowski TL, Moore SS, Cram DJ (1977) J Am Chem Soc 99:2564–2571
2. Kovbasyuk L, Krämer R (2004) Chem Rev 104:3161–3187
3. Pedersen CJ (1967) J Am Chem Soc 89:7017–7036
4. Gokel GW (1991) Crown ethers and cryptands. Royal Society of Chemistry, Cambridge
5. More MB, Glendening ED, Ray D, Feller D, Armentrout PB (1996) J Phys Chem 100:1605–1614
6. Feringa BL (2001) Molecular switches. Wiley-VCH, Weinheim, p 454
7. Balzani V, Scandola F (1991) Supramolecular photochemistry. Ellis Horwood, New York, pp 199–215
8. Liu ZF, Hashimoto K, Fujishima A (1990) Nature 347:658–660
9. Ikeda T, Tsutsumi O (1995) Science 268:1873–1875
10. Sekkat Z, Dumont M (1992) Appl Phys B 54:486–489
11. Hugel T, Holland NB, Cattani A, Moroder L, Seitz M, Gaub HE (2002) Science 296:1103–1106
12. Muraoka T, Kinbara K, Kobayashi Y, Aida T (2003) J Am Chem Soc 125:5612–5613
13. Zhang C, Du MH, Cheng HP, Zhang XG, Roitberg AE, Krause JL (2004) Phys Rev Lett 92:158301(1–4)
14. Halabieh HE, Mermut O, Barrett CJ (2004) Pure Appl Chem 76:1445–1465
15. Shinkai S, Nakaji T, Nishida Y, Ogawa T, Manabe O (1980) J Am Chem Soc 102:5860–5865
16. Tahara R, Morozumi T, Nakamura H, Shimomura M (1997) J Phys Chem B 101:7736–7743
17. Shinkai S, Minami T, Kusano Y, Manabe O (1983) J Am Chem Soc 105:1851–1856
18. Becke AD (1993) J Chem Phys 98:5648–5652
19. Lee C, Yang W, Parr RG (1988) Phys Rev B 37:785–789
20. Korth HG, De Heer MI, Mulder P (2002) J Phys Chem A 106:8779–8789
21. Johnson BG, Gill PMW, Pople JA (1993) J Chem Phys 98:5612–5626
22. Chowdhury PK (2003) J Phys Chem A 107:5692–5696
23. Chis V (2004) Chem Phys 300:1–11
24. Asensio A, Kobko N, Dannenberg JJ (2003) J Phys Chem A 107:6441–6443
25. Müller A, Losada M, Leutwyler S (2004) J Phys Chem A 108:157–165
26. Goncalves NS, Cristiano R, Pizzolatti MG, da Silva Miranda F (2005) J Mol Struct 733:53–61
27. Frisch MJ, Trucks GW, Schlegel HB, Scuseria GE, Robb MA, Cheeseman JR, Montgomery JAJr, Vreven T, Kudin KN, Burant JC, Millam JM, Iyengar SS, Tomasi J, Barone V, Mennucci B, Cossi M, Scalmani G, Rega N, Petersson GA, Nakatsuji H, Hada M, Ehara M, Toyota K, Fukuda R, Hasegawa J, Ishida M, Nakajima T, Honda Y, Kitao O, Nakai H, Klene M, Li X, Knox JE, Hratchian HP, Cross JB, Adamo C, Jaramillo J, Gomperts R, Stratmann RE, Yazyev O, Austin AJ, Cammi R, Pomelli C, Ochterski JW, Ayala PY, Morokuma K, Voth GA, Salvador P, Dannenberg JJ, Zakrzewski VG, Dapprich S, Daniels AD, Strain MC, Farkas O, Malick DK, Rabuck AD, Raghavachari K, Foresman JB, Ortiz JV, Cui Q, Baboul AG, Clifford S, Cioslowski J, Stefanov BB, Liu G, Liashenko A, Piskorz P, Komaromi I, Martin RL, Fox DJ, Keith TM, Al-Laham A, Peng CY, Nanayakkara A, Challacombe MP, Gill MW, Johnson B, Chen W, Wong MW, Gonzalez C, Pople JA (2003) Gaussian 2003W, revision B.05. Gaussian Inc., Pittsburgh
28. Reed AE, Curtiss LA, Weinhold F (1988) Chem Rev 88:899–926
29. Reed AE, Weinhold F (1983) J Chem Phys 78:4066–4073
30. Foster JP, Weinhold F (1980) J Am Chem Soc 102:7211–7218
31. Reed AE, Weinstock RB, Weinhold F (1985) J Chem Phys 83:735–746
32. Schulze FW, Petrick HJ, Cammenga HK, Klinge H (1977) Z Phys Chem Neue Fol 107:4743
33. Cattaneo P, Persico M (1999) Phys Chem Chem Phys 1:4739–4743
34. Ishikawa T, Noro T, Shoda TJ (2001) Chem Phys 115:7503–7512
35. Tiago ML, Ismail-Beigi S, Louie SG (2005) J Chem Phys 122:094311(1–7)
36. Cembran A, Bernardi F, Garavelli L, Gagliardi L, Orlandi G (2004) J Am Chem Soc 126:3234–3243
37. Biswas N, Umpathy S (1997) J Phys Chem 107:7849–7858
38. Mostad A, Romming C (1971) Acta Chem Scand 25:3561–3568
39. Fliegl H, Kohn A, Hattig C, Ahlrichs R (2003) J Am Chem Soc 125:9821–9827
40. Hopkins HP Jr, Norman AB (1980) J Phys Chem 84:309–314
41. Smetana AJ, Popov AI (1980) J Solution Chem 9:183–196
42. Lamb JD, Izatt RM, Swain CS, Christensen JJ (1980) J Am Chem Soc 102:475–479
43. Ouchi M, Inoue Y, Kanzaki T, Hakushi T (1984) J Org Chem 49:1408–1412
44. Pedersen C (1970) J Am Chem Soc 92:391–394
45. Liu Y, Lu TB, Tan MY, Hakushi T, Inoue Y (1993) J Phys Chem 97:4548–4551
46. Ouchi M, Inoue Y (1985) Bull Chem Soc Jpn 58:525–530
47. Ouchi M, Inoue Y, Kanzaki T (1984) Bull Chem Soc Jpn 57:887–888
48. Hill SE, Feller D (2000) Int J Mass Spectrom 201:41–58
49. Adamovic I, Gordon MS (2005) J Phys Chem A 109:1629–1636
50. Mo Y, Wu W, Song L, Lin M, Zhang Q, Gao J (2004) Angew Chem Int Ed 43:1986–1990
51. Mo Y, Jiao H, Schleyer PvR (2004) J Org Chem 69:3493–3499
52. Mo Y, Schleyer PvR, Wu W, Lin M, Zhang Q, Gao J (2003) J Phys Chem A 107:10011–10018
53. Cramer CJ (2002) Essentials of computational chemistry: theories and models, 2nd edn. Wiley, New York
54. Kim KS, Tarakeshwar P, Lee JY (2000) Chem Rev 100:4145–4186
55. Boys SF, Bernardi F (1970) Mol Phys 19:553–566
56. Crecca CR, Roitberg AE (2006) J Phys Chem A 110:8188–8203
57. Nägele T, Hoche R, Zinth W, Wachtveitl J (1997) Chem Phys Lett 272:489–495